

Dynamic Quantum Isotope Effects on Multiple Proton-Transfer Reactions

Yasuteru Shigeta,*[1] Hideaki Miyachi,[2] Toru Matsui,[2] and Kimihiko Hirao[2]

[1]Department of Physics, Graduate School of Pure and Applied Sciences, Tsukuba University, 1-1-1 Tennodai, Tsukuba 305-0006

[2]Department of Applied Chemistry, School of Engineering, The University of Tokyo, 7-3-1 Hongo, Bunkyo-ku, Tokyo 113-8656

Received March 7, 2008; E-mail: shigeta@sci.u-hyogo.ac.jp

In order to investigate static quantum isotope effects on the stability of proton-transferred structures, we defined an effective quantal potential energy hypersurface (EQPES), which includes mass-dependent quantum effects. We demonstrated the difference between the ordinary potential energy surface and EQPES of the double well potential as a simple example. The minimum energy path on EQPES describes the zero-point energy-corrected structures and tunneling motion, which is characterized as a classically forbidden motion. We also performed the EQPES analysis of model proton-transfer reactions in DNA base pairs. It was found that the double proton-transferred structure of an adenine–thymine (AT) pair is quantum mechanically unstable and that of a guanine–cytosine (GC) pair is stable within a least uncertainty regime. In order to investigate dynamic quantum isotope effects on the stability of the proton-transferred structures, we performed quantal cumulant dynamics (QCD) simulations of the GC pair. Results show that the proton-transferred structure of the protonated isotopomer is dynamically unstable though the EQPES analysis predicts its stability. It is relevant to include dynamic effects in the investigation of the quantum isotope effects on geometric stability of systems with a small energy gap between global and metastable structures.

Isotope effects play important roles in chemistry, physics, and biology, because these are strongly related to changes in properties, reaction activities, and isotope ratios in materials, which can be detected in experiments.[1–4] Origins of the isotope effects are due mainly to differences in mass of the nuclei, and in the electronic structure of the system, which is affected by electron–phonon interaction. For example, remarkable isotope effects are found at transition temperatures of superconductors[5,6] and ferroelectrics such as KH_2PO_4,[7] in vibrational spectra of molecules, and in velocities of chemical reactions. The transition temperature of superconductors depends on mass, because the driving force of superconductivity under BCS theory is electron–phonon interaction, which reflects to lattice vibrations of the superconductor.[8,9] In general, the transition temperature increases as mass becomes lighter. The opposite behavior is found in the ferroelectrics. The enhancement of the ferroelectric to antiferroelectric phase transition temperature of KD_2PO_4 ($T_c = 229$ K) over that of KH_2PO_4 ($T_c = 122$ K) is significant. Such enhancement is mainly due to quantum effects on nuclei, which affect both geometric properties of the crystal and electronic structure of the system.

The isotope effects on chemical reactions have been investigated over decades.[10,11] When one substitutes a specific atom into its isotopomer the binding energy is different due to a difference in zero-point energy. In general, the reaction becomes slower as the mass becomes heavier, because the binding energy becomes larger. This phenomenon is well known as the kinetic isotope effect, which is distinguished from equilibrium or geometric isotope effects. The ratio of the kinetic isotope effect is inversely proportional to the square root of the ratio of the mass, i.e. $k_1/k_2 \approx (m_2/m_1)^{1/2}$. Therefore, one of the most prominent isotope effects is observed when a proton is substituted by tritium, $k_T/k_H \approx 0.5774$, or by deuterium, $k_D/k_H \approx 0.7071$, which are much smaller than the ratio of heavy atoms such as oxygen $^{16}O/^{18}O$, $k_{16O}/k_{18O} \approx 0.9428$. Moreover quantum effects such as tunneling enhance the behavior of the isotope effects by the expected ratio. Anomalously large enhancement of heavy isotopes in stratospheric ozone has been found by Mauersberger et al.[12–15] The $^{16}O/^{18}O$ isotope effect on a kinetic constant is about 65%, which is much smaller than the expected value from $k_{16O}/k_{18O} \approx 0.9428$. Similar behavior is observed for NO + O reactions.[16] Recently, the origin of the anomalous isotope effects has been explained by means of quantum scattering theory by Babikov et al. and independently by Xie and Bowman.[17–19] They revealed the zero-point energy of O_2 molecules as playing a key role. Thus, quantum effects are quite important in the isotope effects not only of light mass nuclei, but also of heavy mass nuclei.

Quantum isotope effects have been extensively studied over the decades.[20–27] There are a number of approaches that can be used to treat these quantum effects, at least approximately, such as semiclassical dynamics methods[27–41] and wave function based method.[42–69] We have developed wave function based methods with a simultaneous treatment of electrons and nuclei quantum mechanically.[42–44] Several groups developed and applied these methods to treat static quantum isotope effects on proton/deuteron (H/D) substitutions and proton tunneling.[45–69] Nevertheless it costs too much not to treat

Published on the web October 10, 2008; doi:10.1246/bcsj.81.1230

large-scale systems and it looses the concept of reaction paths of chemical reactions. Dynamic effects such as fluctuation are key issues even in classical dynamics, since observed properties sometimes strongly depend on transitions among many structures. One of us demonstrated that a gigantic charge fluctuation is presented in confined systems such as metallo-endohedral fullerenes.[70] The dynamic effects are also indispensable for investigating quantum nature at low temperature. In particular, dynamic quantum effects such as tunneling and decoherence affect the stability of structures. One of the quite distinguished works to treat dynamic quantum effects with lower cost is the quantized Hamilton dynamics (QHD) approach, which Prezhdo and co-workers developed based on the Heisenberg's equations of motion.[71–76] Several approximations were derived for the evolution of relevant expectation values in the Heisenberg representation. Recently we have developed quantal cumulant dynamics (QCD) as an extension to QHD.[77–79] In this formalism, coordinates, momenta and cumulants are central variables in contrast to QHD. The key ideas are that a coordinate shift operator acting on a potential operator is introduced and that a cumulant expansion is applied to evaluate the expectation value of the shift operator. The advantages of the QCD approach over the QHD method are: (i) a systematic construction of higher-order equations of motion is possible; (ii) there are no errors in the energy and its gradient due to the truncation of the potential; and (iii) there is no tedious derivation with respect to the decomposition scheme in the QHD method.

In this paper, we derive coupled equations of motion of cumulants that consist of symmetric-ordered products of the coordinate and the momentum fluctuation operators. The equations of motion of the second-order cumulants and the expectation values of the coordinate and the momentum operators are given in Section 2. We will introduce an effective quantal potential energy hypersurface, which describes both zero point energy correction and tunneling path. An example of double well potential will be illustrated. In Section 3, we apply both static effective quantal potential energy surface analysis and QCD simulation to the model multiple proton/hydrogen-transfer reactions, i.e. proton/hydrogen-transfer reaction of DNA bases such as three hydrogen bonds in a guanine–cytosine pair and two hydrogen bonds in an adenine–thymine pair. We focus on the static and dynamical stability of its isotopomers. Section 4 provides our conclusions.

Theoretical Background

The Hamiltonian of a multi-dimensional system is given by

$$\hat{H} = \sum_i \frac{\hat{\mathbf{P}}_i^2}{2M_i} + V(\{\hat{\mathbf{Q}}_i\}) \tag{1}$$

where the first term denotes the kinetic energy operator and the second term denotes the potential energy operator. These are functions of momentum operators and mass of the i-th particle and coordinate operators. Those fulfill the commutation relations

$$\begin{aligned} &[\hat{\boldsymbol{Q}}_{ik}, \hat{\boldsymbol{P}}_{jl}] = i\hbar\delta_{ij}\delta_{kl} \\ &[\hat{\boldsymbol{Q}}_{ik}, \hat{\boldsymbol{Q}}_{jl}] = [\hat{\boldsymbol{P}}_{ik}, \hat{\boldsymbol{P}}_{jl}] = 0 \end{aligned} \tag{2}$$

In order to evaluate energy, one generally needs a wave function of the system. Instead, we here use expectation values of functions of coordinate and momentum operators. To do so, we here introduce a coordinate shift operator, defined as

$$V(\{\hat{\mathbf{Q}}_i\}) = \exp\left(\sum_i \delta\hat{\mathbf{Q}}_i \cdot \frac{\partial}{\partial \mathbf{q}_i}\right) V(\mathbf{q}_i)\Big|_{\mathbf{q}_i=\langle\hat{\mathbf{Q}}_i\rangle} \tag{3}$$

where $\delta\hat{\mathbf{Q}}_i = \hat{\mathbf{Q}}_i - \langle\hat{\mathbf{Q}}_i\rangle$ is a fluctuation operator and $\mathbf{q}_i = \langle\hat{\mathbf{Q}}_i\rangle$ is a vector of an expectation value of the i-th coordinate operator. By using the definition and a cumulant expansion technique for central moments, we have

$$\tilde{V}(\{\mathbf{q}_i\}, \{\lambda_{\mathbf{m}_i,\mathbf{0}_i}\}) = \exp\left(\sum_i \sum_{\mathbf{m}_i}^{\infty} \frac{\lambda_{\mathbf{m}_i,\mathbf{0}_i}}{\mathbf{m}_i!} \cdot \frac{\partial^{\mathbf{m}_i}}{\partial \mathbf{q}_i^{\mathbf{m}_i}}\right) V(\mathbf{q}_i) \tag{4}$$

where the tilde denotes the expectation value. Hereafter we abbreviate the limit $\mathbf{q}_i = \langle\hat{\mathbf{Q}}_i\rangle$ for simplicity. In the above equation we have introduced a set of cumulants $\{\lambda_{\mathbf{m}_i,\mathbf{n}_i}\}$, which is m-th- and n-th-order with respect to i-th coordinate and momentum operators, respectively. All cumulants are evaluated in a well-defined manner. In this study, we restrict ourselves on keeping it up to second-order as

$$\tilde{V}_2(\{\mathbf{q}_i\}, \{\lambda_{\mathbf{2}_i,\mathbf{0}}\}) = \exp\left(\sum_i \sum_{k=x,y,z} \frac{\lambda_{2_{ik},0_{ik}}}{2} \frac{\partial^2}{\partial q_{ik}^2}\right) V(\mathbf{q}_i) \tag{5}$$

We call it the second-order quantal potential. By applying the same manner to the kinetic energy term, the total energy within the second-order cumulant theory is written as

$$\begin{aligned} &E_2(\{\mathbf{q}_i\}, \{\mathbf{p}_i\}, \{\lambda_{\mathbf{2}_i,\mathbf{0}}\}, \{\lambda_{\mathbf{0},\mathbf{2}_i}\}) \\ &\quad = \sum_i \frac{\mathbf{p}_i^2 + \lambda_{\mathbf{0},\mathbf{2}_i} \cdot \mathbf{1}}{2M_i} + \tilde{V}_2(\{\mathbf{q}_i\}, \{\lambda_{\mathbf{2}_i,\mathbf{0}}\}) \end{aligned} \tag{6}$$

where we also introduce a vector of the expectation values of the i-th momentum operator, $\mathbf{p}_i = \langle\hat{\mathbf{P}}_i\rangle$, and second-order momentum cumulant variables, $\lambda_{\mathbf{0},\mathbf{2}_i}$. The above expression implies that the energy can be evaluated by means of classical momenta and coordinates and second-order momentum and coordinate cumulant variables.

The cumulant variables are represented by the expectation values of the fluctuation operators as

$$\begin{aligned} \lambda_{\mathbf{2}_i,\mathbf{0}} &= \langle\delta\hat{\mathbf{Q}}_i^2\rangle \\ \lambda_{\mathbf{0},\mathbf{2}_i} &= \langle\delta\hat{\mathbf{P}}_i^2\rangle \end{aligned} \tag{7}$$

To obtain a closed form of coupled equations of motion (EOMs) for $\{\mathbf{q}_i\}$, $\{\mathbf{p}_i\}$, and cumulant variables ($\{\lambda_{\mathbf{2}_i,\mathbf{0}}\}$, $\{\lambda_{\mathbf{0},\mathbf{2}_i}\}$), we here introduce a further second-order cumulant of the product of the momentum and coordinate fluctuation operators defined by

$$\lambda_{\mathbf{1}_i,\mathbf{1}_i} = \langle(\delta\hat{\mathbf{Q}}_i\delta\hat{\mathbf{P}}_i)_s\rangle \tag{8}$$

where s denotes a symmetric-ordered product, i.e. $(\hat{A}\hat{B})_s = \frac{1}{2}(\hat{A}\hat{B} + \hat{B}\hat{A})$. From Heisenberg's equation of motion,

$$\frac{\mathrm{d}}{\mathrm{d}t}\langle\hat{A}(t)\rangle = \frac{1}{i\hbar}\langle[\hat{A}(t), \hat{H}]\rangle \tag{9}$$

we have

$$\begin{aligned} \dot{\mathbf{q}}_i(t) &= \frac{\mathbf{p}_i}{M_i} \\ \dot{\mathbf{p}}_i(t) &= -\frac{\partial}{\partial \mathbf{q}_i}\tilde{V}_2(\{\mathbf{q}_i(t)\}, \{\lambda_{\mathbf{2}_i,\mathbf{0}}(t)\}) \end{aligned}$$

$$\dot{\lambda}_{\mathbf{2}_i,\mathbf{0}}(t) = \frac{2\lambda_{\mathbf{1}_i,\mathbf{1}_i}(t)}{M_i}$$

$$\dot{\lambda}_{\mathbf{1}_i,\mathbf{1}_i}(t) = \frac{\lambda_{\mathbf{0},\mathbf{2}_i}(t)}{M_i} - \lambda_{\mathbf{2}_i,\mathbf{0}} \frac{\partial^2}{\partial \mathbf{q}_i^2} \tilde{V}_2(\{\mathbf{q}_i(t)\}, \{\lambda_{\mathbf{2}_i,\mathbf{0}}(t)\})$$

$$\dot{\lambda}_{\mathbf{0},\mathbf{2}_i}(t) = -2\lambda_{\mathbf{1}_i,\mathbf{1}_i}(t) \frac{\partial^2}{\partial \mathbf{q}_i^2} \tilde{V}_2(\{\mathbf{q}_i(t)\}, \{\lambda_{\mathbf{2}_i,\mathbf{0}}(t)\}) \quad (10)$$

These are central EOMs in QCD theory. If we have N-dimensional systems, the EOMs have $5N$ degrees of freedom. Since the time derivative of the total energy is identically zero, these equations of motion conserve the energy. Moreover we have another set of conserving quantities, $\gamma(t)$, that fulfills $\dot{\gamma}(t) = 0$, where

$$\gamma_{ik}(t) = \lambda_{2_{ik},0}(t)\lambda_{0,2_{ik}}(t) - \lambda^2_{1_{ik},1_{ik}}(t) \quad (11)$$

This implies that the QCD EOMs are redundant so that the actual EOMs have $4N$ degrees of freedom. Nevertheless we have used the $5N$ degrees of freedom in actual calculations, because it does not cost too much and it is easy to handle.

In ordinary potential energy surface (PES) analysis, one pays attention not to the total energy but only to the potential energy. In other words, the kinetic energy is always neglected. In the present work, we have introduced the quantal potential energy in eq 5, which includes quantum effects through the coordinate cumulant variables. With the same idea we can also do the PES analysis. However the momentum cumulant variables are not independent of the coordinate cumulant variables due to the Heisenberg's uncertainty relations. Therefore we should take advantage of the Heisenberg's uncertainty relations as

$$\langle (\delta\hat{\mathbf{Q}}_{ik}\delta\hat{\mathbf{P}}_{ik})_s^2 \rangle = \lambda_{2_{ik},0}\lambda_{0,2_{ik}} + 2\lambda^2_{1_{ik},1_{ik}} \geq \frac{\hbar^2}{4} \quad (12)$$

Assuming the momentum-coordinate cumulants being identically zero, $\lambda_{\mathbf{1}_i,\mathbf{1}_i} = 0$, and a least uncertainty relation, we have

$$\lambda_{0,2_{ik}} = \frac{\hbar^2}{4\lambda_{2_{ik},0}} \quad (13)$$

By substituting the above equation into the energy, one yields

$$E_2^{\mathrm{LU}}(\{\mathbf{q}_i\}, \{\mathbf{p}_i\}, \{\lambda_{\mathbf{2}_i,\mathbf{0}}\}) = \sum_i \frac{\mathbf{p}_i^2}{2M_i} + \sum_i \frac{\hbar^2}{8M_i\lambda_{\mathbf{2}_i,\mathbf{0}}} \cdot \mathbf{1} + \tilde{V}_2(\{\mathbf{q}_i\}, \{\lambda_{\mathbf{2}_i,\mathbf{0}}\}) \quad (14)$$

where LU means the least uncertainty relation and an identity vector defined as $\mathbf{1} = (1, 1, 1)$ has been introduced. The least uncertainty relation reduces the actual variables from $4N$ to $3N$. Again by neglecting the classical kinetic energy we define an effective quantal potential energy hypersurface (EQPES) as

$$\tilde{V}_2^{\mathrm{eff}}(\{\mathbf{q}_i\}, \{\lambda_{\mathbf{2}_i,\mathbf{0}}\}) = \sum_i \frac{\hbar^2}{8M_i\lambda_{\mathbf{2}_i,\mathbf{0}}} \cdot \mathbf{1} + V_2(\{\mathbf{q}_i\}, \{\lambda_{\mathbf{2}_i,\mathbf{0}}\}) \quad (15)$$

The first term originates from a quantum correction to the kinetic energy, which is inversely proportional to the coordinate cumulants and masses. On the other hand, the second term contains a quantum correction to the potential energy, which is a function of both classical coordinates and coordinate cumulant variables. Thus, the quantum isotope effects are consequences due to a competition between the first mass-dependent and the second mass-independent terms. Owing to the first term and the definition of $\lambda_{\mathbf{2}_i,\mathbf{0}}$, $\lambda_{\mathbf{2}_i,\mathbf{0}}$ is always greater than zero, $\lambda_{\mathbf{2}_i,\mathbf{0}} > 0$. If we assume $M_i\lambda_{\mathbf{2}_i,\mathbf{0}}/\hbar^2 \to \infty$ and $\lambda_{\mathbf{2}_i,\mathbf{0}} \to 0$, the EQPES agrees with the ordinary PES (classical limit). This potential is equivalent to that obtained by Gaussian wave packet by Ando to investigate proton-transfer reactions in condensed phases.[26]

Here, we evaluate the density based on the QCD method.[79] The density is defined as the expectation value of the delta function, and then we have

$$\tilde{\rho}(\mathbf{q}_0) = \langle \delta(\hat{\mathbf{Q}} - \mathbf{q}_0) \rangle \quad (16)$$

By using the cumulant expansion techniques, the density can be expressed in terms of an infinite series of the cumulant variables. The second-order density is given by

$$\tilde{\rho}_2(\mathbf{q}_0) = \exp\left(\sum_i \sum_{k=x,y,z} \frac{\lambda_{2_{ik},0_{ik}}}{2} \frac{\partial^2}{\partial q_{ik}^2} \right) \times \lim_{\mathbf{a}\to\infty} \frac{\exp(-(\mathbf{q}-\mathbf{q}_0)^T \cdot \mathbf{a} \cdot (\mathbf{q}-\mathbf{q}_0)^2)}{\sqrt{\prod_i \prod_{k=x,y,z} 2\pi a_{ik}}} \quad (17)$$

where we have used the fact that the delta function can be expressed as the Gaussian with infinite exponent limit. By using the Fourier convolution technique, the density is evaluated as

$$\rho(\mathbf{q}_0) = \frac{1}{\sqrt{\prod_i \prod_{k=x,y,z} 2\pi\lambda_{2_{ik},0_{ik}}}} \times \exp\left(-\sum_i \sum_{k=x,y,z} \frac{(q_{ik} - q_{0,ik})^2}{2\lambda_{2_{ik},0_{ik}}} \right) \quad (18)$$

The density is expressed as a Gaussian function of the classical expectation values, $\{q_{ik}\}$, and the second-order position cumulant, $\{\lambda_{2_{ik},0_{ik}}\}$. The classical expectation values and the second-order cumulant variables correspond to the center and the width of the Gaussian along each direction, respectively. Since the resultant density is given by the Gaussian, the method is almost equivalent to the Gaussian wave packet method by Fiete and Heller.[29] A difference between Heller's and the present approaches is that one does not truncate a given potential by quadratic-order as done by Heller's approach so that the method is applicable to any potential such as the Morse, Coulomb,[77] and quadratic potentials generated from ab initio methods.[76]

An illustrative example we here consider is a one-dimensional symmetric double well potential given as

$$V(q) = aq^4 + bq^2 \quad (19)$$

It is quite easy to derive second-order EQPES as follows:

$$\tilde{V}_2^{\mathrm{eff}}(q, \lambda) = \frac{\hbar^2}{8M\lambda} + aq^4 + (b + 12a\lambda)q^2 + 3a\lambda^2 + \lambda b \quad (20)$$

In Figure 1, we have plotted the minimum energy path from one well to the other. It is smoothly drawn by red dots. Note that the effective potential diverges at $\lambda = 0$ due to the first term, but not specified in the figure. This figure indicates that (i) potential becomes single minimum for $\lambda \gg 1$ (strong quantum case) and double minima for $\lambda \ll 1$ (weak quantum case).

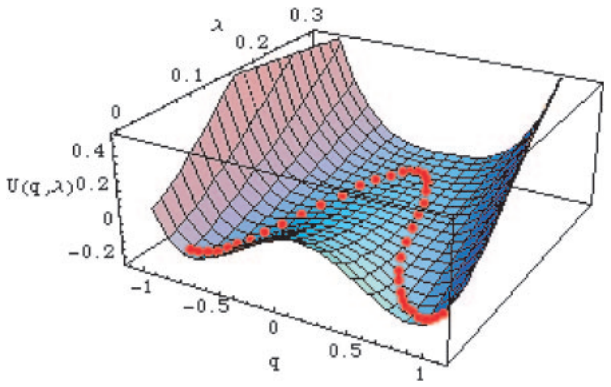

Figure 1. Effective quantal potential energy hypersurface (EQPES) and minimum energy path on it (red dotted line).

The stable geometries and transition state are obtained from variations of the EQPES with respect to the q and λ as

$$\frac{\partial}{\partial q}\tilde{V}_2^{\text{eff}}(q,\lambda) = 4aq^3 + 2(b+12a\lambda)q = 0$$
$$\frac{\partial}{\partial \lambda}\tilde{V}_2^{\text{eff}}(q,\lambda) = -\frac{\hbar^2}{8M\lambda^2} + 6a(q^2+\lambda) + b = 0 \qquad (21)$$

Once parameters a, b, and M are determined, variational solutions of q and λ are evaluated numerically. For example, if we set $a = 0.7$, $b = -1$, and $M = 50\hbar^2$, the global minima are given by $\tilde{E}_{\min,QG}(\pm 0.7736, 0.03863) = -0.221434$ on the EQPES and $E_{\min,C}(\pm 0.8452) = -0.357143$ on the classical PES. We also have a metastable state at the origin and the corresponding energy is $\tilde{E}_{\min,QM}(0, 0.24779) = -0.108761$. On the other hand, the two transition states are $\tilde{E}_{TS,Q}(\pm 0.1285, 0.2326) = -0.108426$. Note that the classical TS is located at the origin and the corresponding energy is zero. Since the minimum energy path passes through the point, which is energetically lower than the classical TS, it reflects a tunneling motion. The energy barrier of the effective tunneling reaction on the EQPES, $\Delta E_Q = 0.113008$, is lower than the classically allowed transition energy (not tunneling motion), $\Delta E_C = 0.357143$. The barrier between TS and the metastable state is negligibly small, $\Delta E_{TS-MS} = 0.000335$. Therefore, the transition from one to the other side is activated with less energy than the classical one needs. This is one of the signatures of a quantum kinetic isotope effects.

Results and Discussion

Model Systems. In this work we consider multiple proton/hydrogen-transfer reactions in DNA bases. The multiple proton-transfer reactions in these systems were investigated by Florián et al. by density functional calculations.[80,81] Later, quantum mechanical treatments for the system were performed by Villani.[82] We also investigated influences of the metal binding to the base pairs and of the staking effects on multiple proton-transfer reactions.[83] We here adopt two models, where one is a two-dimensional model for two hydrogen bonds in an AT pair, and the other is a three-dimensional model for three hydrogen bonds in a GC pair as depicted in Figure 2. In Villani's study, he construct model potentials for the AT and GC pairs given by

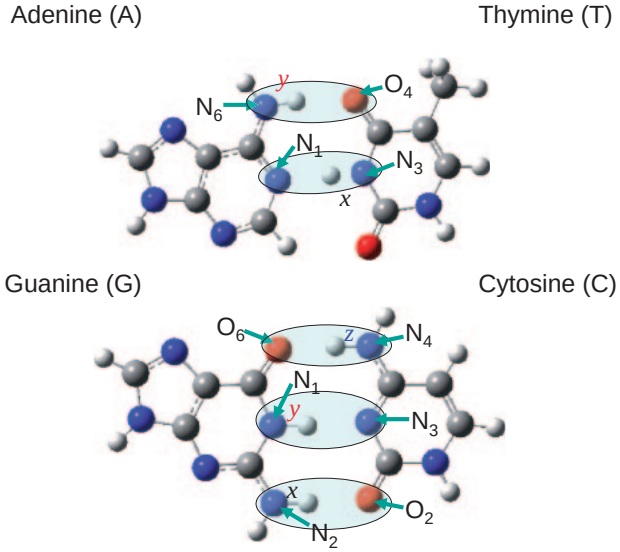

Figure 2. Models for multiple proton-transfer reactions in DNA base pairs. x, y, and z are reaction coordinates of the proton-transfer reactions.

$$V^{AT}(x,y) = \sum_{i,j} h_{i,j}x^i y^j$$
$$V^{GC}(x,y,z) = \sum_{i,j,k} h'_{i,j,k}x^i y^j z^k \qquad (22)$$

where parameters in the model potential are given by Villani's paper, which is sixth- and fifth-order polynomials with respect to the coordinates for AT and GC pairs, respectively, determined by the first principle calculations (B3LYP/cc-pVDZ). The reaction coordinates x, y, and z are shown in the figure. The corresponding quantal potentials are explicitly given by

$$\tilde{V}_2^{AT}(x,y,\xi,\eta) = \sum_{l=0}^{3}\sum_{k=0}^{3}\sum_{i=0}^{6-2l}\sum_{j=0}^{6-2k}\frac{(i+2l)!}{i!l!}\frac{(j+2k)!}{j!k!}h_{i+2l,j+2k}x^i y^j\left(\frac{\xi}{2}\right)^l\left(\frac{\eta}{2}\right)^k \qquad (23)$$

$$\tilde{V}_2^{GC}(x,y,z,\xi,\eta,\zeta) = \sum_{l,m,n=0}^{2}\sum_{i=0}^{5-2l}\sum_{j=0}^{5-2m}\sum_{k=0}^{5-2n}H_{i,j,k}^{l,m,n}x^i y^j z^k\left(\frac{\xi}{2}\right)^l\left(\frac{\eta}{2}\right)^m\left(\frac{\zeta}{2}\right)^n$$
$$H_{i,j,k}^{l,m,n} = \frac{(i+2l)!}{i!l!}\frac{(j+2m)!}{j!m!}\frac{(k+2n)!}{k!n!}h'_{i+2l,j+2m,k+2n} \qquad (24)$$

where Greek characters denote the cumulant variables. When some variables are large, this potential becomes a negatively large value that is less than the minima of interest. In this work we have added extra terms, which prevent particles from escaping from the minima and do not affect the shape of potential energy surface around the minima and TSs. The additional well-like potential is defined as

$$V_{\text{well}}(\{q_i\}) = V_0\left[1 + \prod_{i=x,y,z}(\theta_b(q_i - q_{i\,\max}) - \theta_b(q_i - q_{i\,\min}))\right] \qquad (25)$$

where $q_{i\,\max}$ and $q_{i\,\min}$ are maximum and minimum range of potential and V_0 is height of the well-like potential. An approximate Heaviside function is given by

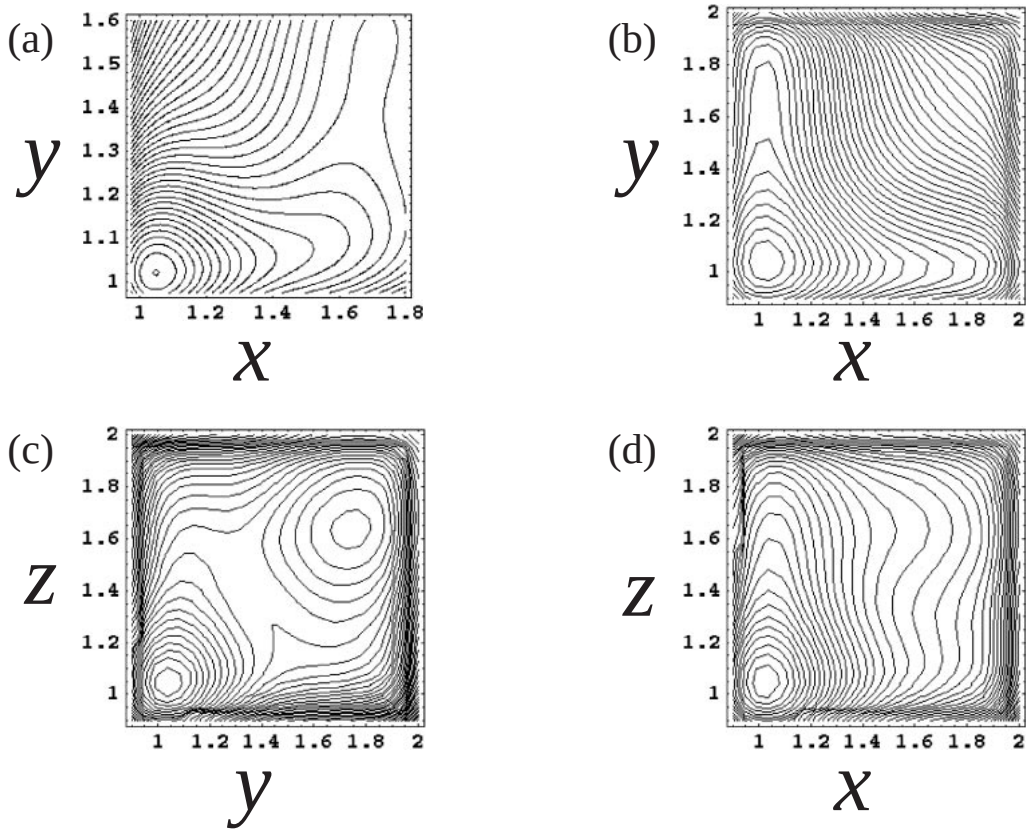

Figure 3. Modified potential energy surfaces of (a) AT pair, (b) x–y plane of GC pair at $z_e = 1.045$, (c) y–z plane of GC pair at $x_e = 1.025$, and (d) x–z plane of GC pair at y–z plane of GC pair at at $y_e = 1.037$.

$$\theta_b(x) = \frac{\mathrm{erf}(\sqrt{b}x) + 1}{2} \tag{26}$$

where b is an effective width of the approximate Heaviside function and guarantees smoothness of the potential. When V_0 is appropriately large, the particles stay around minima during dynamics simulations. In actual calculations we set $b = 100$, $q_{i,\max}/\text{Å} = 2.0$, $q_{i,\min}/\text{Å} = 0.4$, and $V_0/\text{a.u.} = 0.05$. Both $q_{i,\max}$ and $q_{i,\min}$ are in a reasonable range for the coordinate of the proton, because the distances between heavy elements (O and N) of the DNA bases are approximately 2.7–3.0 Å and roughly speaking the bond length of OH and NH are almost 1.0–1.1 Å. We have checked that this additional potential does not affect the energy of the equilibrium geometry and the equilibrium structure. The quantal potential for the well-like potential is analytically given by

$$\begin{aligned}\tilde{V}_{\mathrm{well}}(\{q_i\},\{\lambda_{2i,0}\}) = 1 + V_0 \prod_{i=x,y,z} (&\tilde{\theta}_b(q_i - q_{i\,\max}, \lambda_{2i,0}) \\ &- \tilde{\theta}_b(q_i - q_{i\,\min}, \lambda_{2i,0}))\end{aligned} \tag{27}$$

where the modified quantal Heaviside function is

$$\tilde{\theta}_b(x,\xi) = \frac{\mathrm{erf}(\sqrt{b}x/\sqrt{1+4b\xi}) + 1}{2} \tag{28}$$

The shape of $\tilde{\theta}_b(x,\xi)$ is almost the same, but slightly looser than that of $\theta_b(x)$, because of $1/\sqrt{1+4b\xi} < 1$. The modified PESs are depicted in Figure 3, where we fixed one variable at the equilibrium geometry in order to draw the two-dimensional PES of the GC pair. The ordinary PES analysis gives global minimum and metastable structures both for the AT and GC pairs. The former structure is the ordinary Watson–Crick type (see Figure 2) and the latter is double proton-transferred, as easily found in (a) and (c), where the double proton-transfer reactions occur along the x–y axes for the AT pair and the y–z axes for the GC pair, respectively. No other proton-transferred structure is found on the PES.

Static Case. Here we analyze the EQPES defined above in order to investigate static quantum isotope effects on the proton-transfer reactions. At first we fix the classical variables at the equilibrium geometry on the classical PES, $\{q_{\mathrm{eq},i}\}$, and optimize the cumulant variables on the partially frozen EQPES (fixed geometry search), $\tilde{V}_2(\{q_i\} = \{q_{\mathrm{eq},i}\}, \{\lambda_{2i,0}\})$, and then proceed to fully relaxed geometry search both for the classical and cumulant variables on the EQPES.

We have sketched the EQPES of the AT pair at the fixed geometry for proton and deuteron cases in Figure 4. As the mass increases, the EQPES becomes tight and the cumulant variables at the equilibrium tend to be small. The same situations are observed in the cases of the GC pairs (not shown). These imply that the first term in eq 15 certainly contributes to the equilibrium points. Comparing (a) and (b), the cumulant variables at the equilibrium of (b) are greater than those of (a), because the potentials around the global minimum and the metastable structure are tight and loose, respectively, so that the EQPES takes over the same tendency.

We have plotted densities of the proton and deuteron for the AT pair calculated from eq 18 with variational solutions of the EQPES with respect to $\mathbf{q} = (x, y)$ and $\lambda = (\xi, \eta)$ (Figure 5).

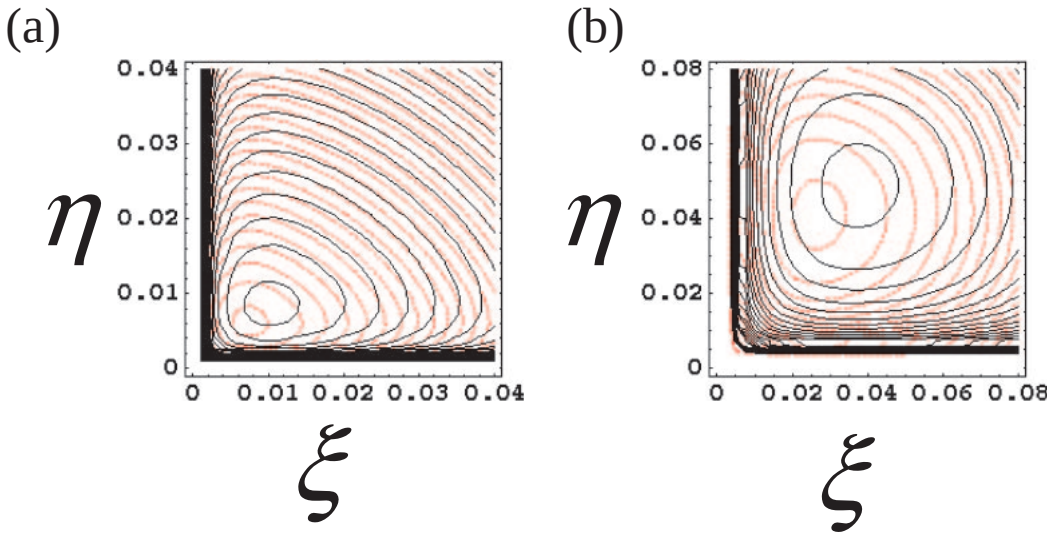

Figure 4. Effective quantal potential energy surfaces of AT pair at (a) global geometry ($x_e = 1.049$ and $y_e = 1.021$) and (b) metastable geometry ($x_e = 1.702$ and $y_e = 1.518$). The black contour is the case of the proton and the red one is the case of the deuteron.

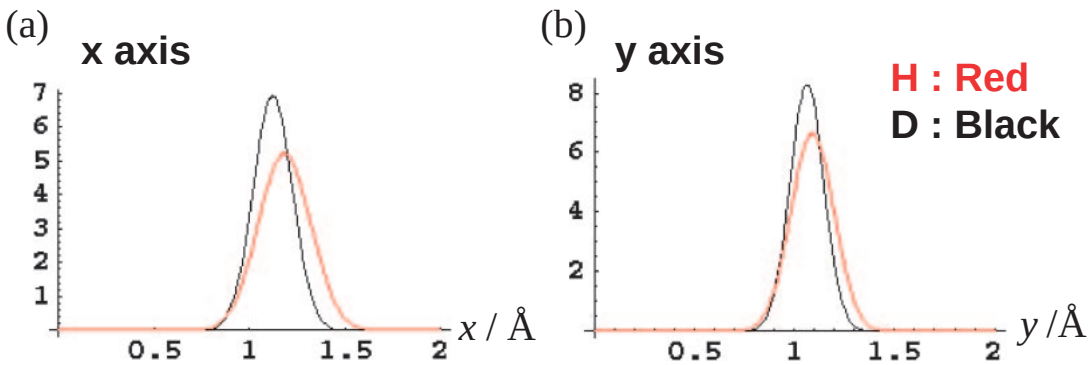

Figure 5. Density of proton (black) and deuteron (red) calculated from the global minimum solution along (a) x and (b) y axis.

We found explicit geometric isotope effects on the density. The density of the proton is broader than that of the deuteron both along x and y axes. In other words, lighter particles tend to delocalize. Centers of density are different from each other. The center of the proton is located at $(x_H, y_H) = (1.184, 1.090)$, on the other hand that of the deuteron is slightly shifted toward shorter distance, $(x_D, y_D) = (1.122, 1.063)$, which are longer than the equilibrium coordinates on the ordinary PES, $(x_{eq}, y_{eq}) = (1.049, 1.021)$. This behavior is also found in results obtained from the wave function-based methods previously done by us for small systems.[42–44] The difference among the centers is intuitively recognized as the difference of the bottom of PES and a quantum mechanical expectation value of the position for example for a hydrogen molecule. The nuclear density is measured directly from neutron diffraction and indirectly from X-ray diffraction experiments for crystals. According to the measurements the same tendencies are found. The geometric isotope effects are consequences of both the delocalization (or localization) of density and the shift of equilibrium positions. These microscopic effects influence not only the structure of small systems but also macroscopic properties such as the phase transition of ferroelectric materials.

Figure 6 depict energy levels of global minima and metastable states as a function of $\log_{10}(M/\text{a.u.})$, where the initial parameters for a geometry search are set around global minima (red) and metastable structure (blue). In contrast with a fixed geometry search, the metastable structure of AT exists when the mass is heavier than $M/\text{a.u.} \approx 10^{6.7}$ and suddenly disappears, because the barrier between the metastable structure and TS is too shallow. The energy gap between two states is $54\,\text{kJ mol}^{-1}$ for the classical case ($\log_{10}(M/\text{a.u.}) = \infty$). These results imply that it is important to perform relaxed geometry search on the EQPES for the quantum isotope effects. Note here that the masses of the proton and deuteron are about 1836 and 3672 a.u., respectively. It indicates that the proton-transferred structure of the AT pairs is unstable both in protonated and deuterated AT pairs. On the other hand, there exist both global and metastable structures in GC pairs for the entire range. The energy gap between the two states is 13, 17, and $50\,\text{kJ mol}^{-1}$ for proton ($\log_{10}(M/\text{a.u.}) = 3.26387$), deuteron ($\log_{10}(M/\text{a.u.}) = 3.56490$), and classical cases ($\log_{10}(M/\text{a.u.}) = \infty$), respectively. If the mass becomes lighter, say in the case of a muon ($\log_{10}(M/\text{a.u.}) = 2.32015$), the gap will disappear. We found explicit isotope effects on the energy gap.

From these EQPES analyses we conclude here that the dou-

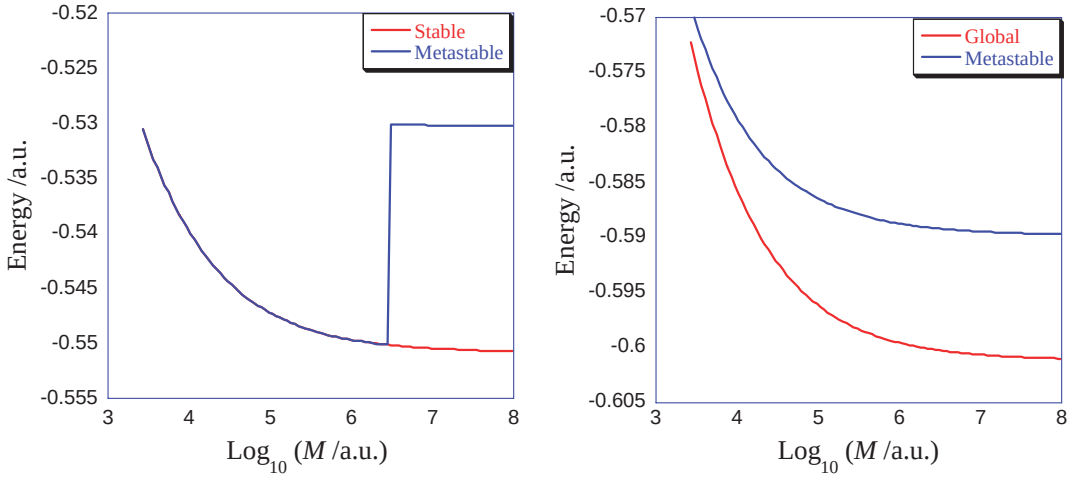

Figure 6. Mass dependency on energy level for (a) AT and (b) GC pairs. The red and blue lines indicate the global and metastable structures at the initial parameters.

ble proton-transferred structure of the AT pair is not stable and that of the GC pair might be stable both for protonated and deuterated cases. Nevertheless the energy gap between global and metastable structures is small enough that thermal activation may drive the proton-transfer reactions from the metastable to global minimum.

Dynamic Case. In order to investigate dynamic stability of proton-transferred structures of the model system, we here perform QCD simulation on the quantal potential. Note here that the above EQPES is one approximation to the effective potential with $2N$ degrees of freedom to the QCD phase space with $4N$ degrees of freedom. Therefore, QCD phase space analysis is a more rigorous way to understand the stability of the proton-transferred structures. Since in the previous paragraph we have shown that the proton-transferred structures of the ordinary GC and its deuterated isotopomer are stable based on the EQPES analysis, we here treat the GC pair. In order to solve the EOMs of eq 10, the time interval used was 0.1 fs, total time was 2 ps, and a fourth-order Runge–Kutta integrator was used in our simulations. The initial conditions of the variables can be determined as

$$\begin{aligned} \mathbf{q}_i(0) &= \min[V(\{\mathbf{q}_i\})] \\ \mathbf{p}_i(0) &= 0 \\ \lambda_{\mathbf{2}i,\mathbf{0}i}(0) &= \min[\tilde{V}_2^{\mathrm{eff}}(\{\mathbf{q}_i\} = \{\mathbf{q}_i(0)\}, \lambda_{\mathbf{2}i,\mathbf{0}i})] \\ \lambda_{\mathbf{0}i,\mathbf{2}i}(0) &= \frac{\hbar^2}{4M_i\lambda_{\mathbf{2}i,\mathbf{0}i}(0)} \\ \lambda_{\mathbf{1}i,\mathbf{1}i}(0) &= 0 \end{aligned} \tag{29}$$

In order to estimate the initial conditions, one needs to search the point that satisfies the least quantal energy principle. In Figure 7 we have depicted phase space $(x/p_x, y/p_y, z/p_z)$ structures of a trajectory obtained by the QCD simulations. For cases (a) and (b), the dynamic feature of the closed orbits is the same except for its amplitudes. The phase space of the x/p_x is compact, on the other hand, that of z/p_z is loose in comparison with that of y/p_y. The explicit isotope effects on the phase space structure are found in the cases of (c) and (d). In Figure 7c, the nuclei initially located at the metastable structure go out from the basin and strongly vibrate around the global minimum due to tunneling. On the other hand, the deuterated isotopomer remains around the metastable structure. It is concluded that the metastable structure of the protonated isotopomer is dynamically unstable, though it is statically stable based on the EQPES analysis. Therefore, it is important to take the dynamical effects into quantum isotope effects on the metastable structure with a small energy gap.

Discussion. Here we discuss open questions in the present QCD-based theories and strategies to tackle them. In this study, we have focused on the stability of global and metastable structures. The EQPES analyses and QCD simulations of the proton-transfer reactions in DNA pairs were performed, since the H/D geometric quantum isotope effects are remarkable due to tunneling and large mass difference. One of the issues, which should be treated by quantum mechanics, is molecular vibration. Since we have defined a new effective potential (EQPES), which includes quantum effect through extended variables, we can consider vibrational analysis of the EQPES. In particular, positive and negative frequencies of the resultant normal modes are related to vibrational frequencies and useful to detect TSs, respectively. According to ordinary normal mode analysis (NMA), a set of N vectors, which consist of only classical coordinates, is evaluated by diagonalizing a Hessian matrix (second derivative matrix) of the PES. By analogy of the ordinary procedure, we may define normal modes, which consist of both classical coordinates and coordinate cumulant variables, by diagonalizing the Hessian matrix evaluated from the EQPES. Because the actual variables in the present theory are $2N$, we result in $2N$ normal modes, which are different from those in the ordinary NMA. Nevertheless a quantum correction to the ordinary normal modes is expected to be small. We performed the QCD simulations of given normal mode Hamiltonian obtained by three-mode quartic force field method,[41,84,85] which contains anharmonic terms. From the results, we found that the QCD simulations give better vibrational frequencies than classical dynamics simulations do. In those cases, the quantum correction to the vibrational frequency is at most 60 cm^{-1} for small molecules, which is small enough to treat as perturbations. Therefore we may find quantum-correct-

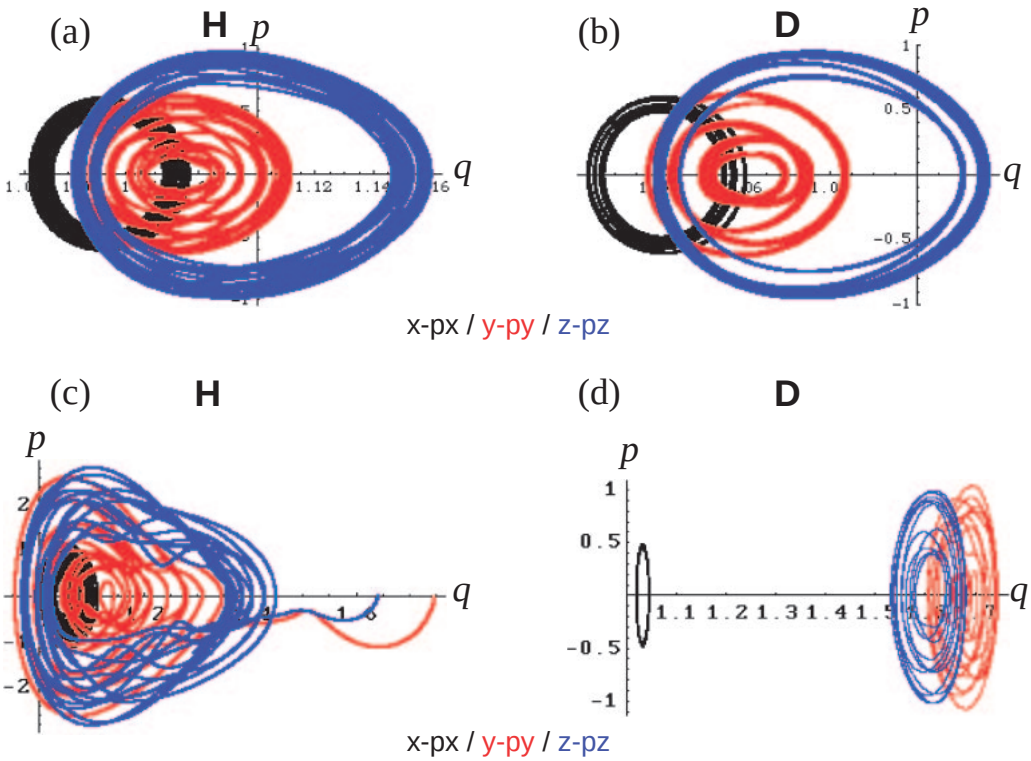

Figure 7. QCD phase space structures of the GC pair, where $q = x$, y, or z and $p = p_x$, p_y, or p_z, respectively. (a) and (b) are initially located around the global minimum for the protonated and deuterated cases. (c) and (d) are initially located around the metastable structure for the protonated and deuterated cases.

ed vibrational modes from the normal modes that have dominant component in the classical coordinates.

For example we apply the extended NMA to the one-dimensional Morse Oscillator based on QCD. Since the dimensions of the cumulant variables are different from those of classical ones, we should introduce alternative variables in order to consider the combined normal coordinates that consist of q and $\lambda_{2,0}$. The coordinate and conjugate momentum are given by

$$\begin{aligned} q_\lambda &= \sqrt{\lambda_{2,0}} \\ p_\lambda &= \lambda_{1,1}/\sqrt{\lambda_{2,0}} \end{aligned} \tag{30}$$

where the dimensions of q_λ and p_λ are the same as those of q and p. The effective energy for the one-dimensional system is evaluated as

$$\begin{aligned} &\tilde{E}_{\mathrm{eff}}(q, p, q_\lambda, p_\lambda) \\ &\quad = \frac{p^2}{2M} + \frac{p_\lambda^2}{2M} + \frac{1}{8Mq_\lambda^2} + \exp\left(\frac{q_\lambda^2}{2}\frac{\partial^2}{\partial q^2}\right) V_M(q) \end{aligned} \tag{31}$$

where $V_M(q) = D_e(e^{-2\alpha(q-q_{eq})} - 2e^{-\alpha(q-q_{eq})})$ is the Morse potential. The Morse potential has three characteristic parameters, D_e, α, and q_{eq}, which correspond to the dissociation energy, curvature, and the equilibrium distance in the molecular vibration of diatomic systems. We set, $D_e = \alpha = q_{eq} = 1$ in this study. The second and third terms in eq 31 arise from an assumption from eq 11, $\gamma = \lambda_{2,0}\lambda_{0,2} - \lambda_{1,1}^2 = \hbar^2/4$, which is compared with the uncertainty relation, $\lambda_{2,0}\lambda_{0,2} + 2\lambda_{1,1}^2 \geq \hbar^2/4$. By means of the Taylor series expansion, the effective energy is approximately given by second-order with respect to q and q_λ as

$$\begin{aligned} \tilde{E}_{\mathrm{eff}}(q, p, q_\lambda, p_\lambda) &\approx \frac{1}{2M}\begin{pmatrix} p & p_\lambda \end{pmatrix}\begin{pmatrix} p \\ p_\lambda \end{pmatrix} \\ &+ \frac{1}{2}\begin{pmatrix} \bar{q} & \bar{q}_\lambda \end{pmatrix}\begin{pmatrix} \tilde{V}_{qq} & \tilde{V}_{q\lambda} \\ \tilde{V}_{q\lambda} & \tilde{V}_{\lambda\lambda} \end{pmatrix}\begin{pmatrix} \bar{q} \\ \bar{q}_\lambda \end{pmatrix} + \tilde{V}_{0,\mathrm{eff}} \end{aligned} \tag{32}$$

where we have used the following abbreviations as

$$\begin{aligned} \bar{q} &= q - q_{\mathrm{opt}} \\ \bar{q}_\lambda &= q_\lambda - q_{\lambda,\mathrm{opt}} \end{aligned} \tag{33}$$

and

$$\begin{aligned} \tilde{V}_{qq} &= \left.\frac{\partial^2 \tilde{V}_2^{\mathrm{eff}}(q, q_\lambda^2)}{\partial q^2}\right|_{q=q_{\mathrm{opt}}, q_\lambda = q_{\lambda,\mathrm{opt}}} \\ \tilde{V}_{q\lambda} &= \left.\frac{\partial^2 \tilde{V}_2^{\mathrm{eff}}(q, q_\lambda^2)}{\partial q \partial q_\lambda}\right|_{q=q_{\mathrm{opt}}, q_\lambda = q_{\lambda,\mathrm{opt}}} \\ \tilde{V}_{\lambda\lambda} &= \left.\frac{\partial^2 \tilde{V}_2^{\mathrm{eff}}(q, q_\lambda^2)}{\partial q_\lambda^2}\right|_{q=q_{\mathrm{opt}}, q_\lambda = q_{\lambda,\mathrm{opt}}} \end{aligned} \tag{33}$$

$\tilde{V}_{0,\mathrm{eff}}$ is the energy at equilibrium geometry. The optimized coordinates, q_{opt} and $q_{\lambda,\mathrm{opt}}$, are obtained from the variational solutions of EQPS. By diagonalizing the matrix in eq 32, one yields vibrational frequencies based on the extended NMA on EQPS, where the lower energy solution corresponds to the corrected vibrational frequency over that obtained from the ordinary NMA. Figure 8 depicts frequencies obtained from the ordinary NMA on PES and from the extended NMA on EQPS as a function of the mass. We also plotted the energy

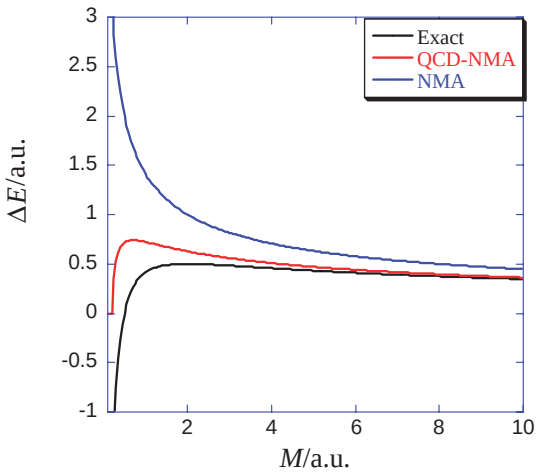

Figure 8. Energy gap between the ground and first excited states estimated from the exact solution (Black). The frequencies obtained from the extended NMA on the EQPS (Red) and from the ordinary NMA (Blue) are also depicted.

gap between the ground and the first excited state estimated from the exact solution. The behavior of the exact solution is that (i) there exists a peak around M/a.u. ≈ 1 and (ii) the energy gap becomes negative for M/a.u. < 0.5 which is a lower boundary for the existence of the first excited state. The extended NMA gives more accurate results than the ordinary NMA does. Although the result by the extended NMA is unfortunately inaccurate for M/a.u. < 5 by comparing with the exact result, its behavior is similar. The frequency becomes complex for less than M/a.u. ≈ 0.2. This behavior corresponds to the inexistence of the first excited state. On the other hand, the ordinary NMA does not have any peak and always exists in the first excited state. Therefore the extended NMA gives reasonable correction to the results obtained from the ordinary NMA as expected. The detailed extension of the NMA on EQPES and its application are given elsewhere.

We did not consider here thermal effects explicitly. In ordinary MD simulations and PES analyses, one can treat thermal properties based on Boltzmann weighted expectation values. In 1932, Wigner derived a sophisticated quantum correction term to thermodynamic properties.[86] Later Feynman and Hibbs developed an effective potential approach derived from a variational method based on a path integral formalism.[87,88] The correction term resembles a term appearing in the quantal potential, where the position cumulant variables are taken by mass- and temperature-dependent variables. Winstead et al. checked the applicability of several quantum correction terms for describing an electron in a semiconductor device.[89] In relation to the present theory, Prezhdo has pointed out that the thermodynamic beta ($\beta = 1/k_{\mathrm{B}}T$) in the Boltzmann factor is modified to be half in the QHD- (or QCD-) based statistical dynamics for the harmonic oscillator.[73] The reason why the half factor appears is that one needs to deal with double variables in the QHD- and QCD-based theories. Nevertheless it is not true for the general cases, since it holds only for the harmonic oscillator. Horikoshi also derived a weight factor from modified Nambu's generalized Hamiltonian mechanics,[90,91] where he used three independent variables as a canonical triplet (x, y, and z), which are related to the present variables as $x = q^2 + \lambda_{2,0}$, $y = p^2 + \lambda_{0,2}$, and $z = \lambda_{1,1}$. Nevertheless in this formulation an ambiguity in the definition of the weight factor remains. Therefore it is expected to construct correct quantum mechanical thermodynamic Boltzmann weight. One possible solution to include thermal effects is to adopt the Nosé–Hoover thermostat method. We have checked that the thermostat variable couples not the whole variables but the classical coordinates and momenta. Other possibility is to use a path integral formulation of the weight factor, which is often used in the standard path integral molecular dynamics (PIMD) methods, as done by Feynman. A difference between the standard and the present theory is that a zero-order trajectory of the standard PIMD is obtained from classical mechanics and that of the present is from the QCD, which includes quantum correction a bit. Theoretical developments and applications of these methodologies will be given in future work.

Conclusion

We have formulated quantal cumulant dynamics (QCD) in order to investigate quantum isotope effects on dynamics. From the least uncertainty relation, quantum correction to the kinetic energy is expressed by means of the coordinate cumulant variables. The correction term is mass-dependent so that we have a mass-dependent effective quantal potential for the analysis of static quantum isotope effect.

We have demonstrated how different the ordinary PES and EQPES are. When the quantum effect is strong (large coordinate cumulant limit $\lambda_{2,0} \to \infty$), the EQPES of a double well potential has a single minima. On the other hand there exist two minima for the weak quantum region (small coordinate cumulant $\lambda_{2,0} \ll 1$). The energy barrier becomes lower due to a zero-point energy correction, and consequently tunneling motion is allowed.

We have numerically shown the geometric isotope effects on the stability of the proton-transferred structures of DNA base pairs as a function of the mass. In particular, a static metastable state, that is found in classical PES, disappears as the mass becomes lighter for the AT pair. On the other hand, there exist static metastable double proton-transferred states even both for protonated and deuterated isotopomers for the GC pair. This is because the barrier height between TS and metastable state is expected to be quite shallow for the AT and relatively deep for the GC pair, respectively. We have performed QCD simulations in order to investigate dynamic stability of the proton-transferred GC pair. The results showed that the proton-transferred structure of the protonated isotopomer is dynamically unstable and that of deuterated isotopomer remains stable. In the former case, dynamically induced transition from the metastable to global minimum occurs. It is relevant to include dynamic effects to treat quantum isotope effects in proton-transfer reactions.

The authors thank Prof. Villani for providing parameter sets of potential energy surfaces for AT and GC pairs. This research was supported by the Core Research for Evolutional Science and Technology (CREST) Program "High Performance Computing for Multi-Scale and Multi-Physics Phenomena" of the Japan Science and Technology Agency (JST).

References

1 P. F. Cook, *Enzyme Mechanism from Isotope Effects*, CRC press inc., **1991**; A. Kohen, H. U. Limbach, Isotope Effects in Chemistry & Biology, CRC press inc., **2006**.

2 V. G. Plekhanov, Isotope Effects in Solid State Physics, Academic press, NY, **2001**.

3 V. G. Plekhanov, *Giant Isotope Effect in Solids*, S.-University Press, La Jolla, USA, **2004**.

4 V. G. Plekhanov, *Applications of the Isotopic Effect in Solids*, Springer, Berlin, **2004**.

5 E. Maxwell, *Phys. Rev.* **1950**, *78*, 477.

6 C. A. Reynolds, B. Serin, W. H. Wright, L. B. Nesbitt, *Phys. Rev.* **1950**, *78*, 487.

7 Y. Tominaga, M. Tokunaga, *J. Crystallogr. Soc. Jpn.* **1998**, *40*, 26.

8 J. Bardeen, L. N. Cooper, J. R. Schrieffer, *Phys. Rev.* **1957**, *108*, 1175.

9 G. Rickayzen, *Theory of Superconductivity*, Wiley, New York, **1964**.

10 L. Melander, *Isotope Effects on Reaction Rates*, New York, Ronald, **1960**.

11 L. Melander, W. H. Saunders, Jr., *Reaction Rates of Isotopic Molecules*, New York, Wiley, **1980**.

12 K. Mauersberger, *Geophys. Res. Lett.* **1981**, *8*, 935.

13 S. M. Anderson, D. Hülsebusch, K. Mauersberger, *J. Chem. Phys.* **1997**, *107*, 5385.

14 K. Mauersberger, B. Erbacher, D. Krankowsky, J. Günther, R. Nickel, *Science* **1999**, *283*, 370.

15 C. Janssen, J. Guenther, K. Mauersberger, D. Krankowsky, *Phys. Chem. Chem. Phys.* **2001**, *3*, 4718.

16 H. Umemoto, K. Tanaka, S. Oguro, R. Ozeki, M. Ueda, *Chem. Phys. Lett.* **2001**, *345*, 44.

17 D. Babikov, B. K. Kendrick, R. B. Walker, R. Schinke, R. T. Pack, *Chem. Phys. Lett.* **2003**, *372*, 686.

18 D. Babikov, B. K. Kendrick, R. B. Walker, R. T. Pack, P. Fleurat-Lesard, R. Schinke, *J. Chem. Phys.* **2003**, *119*, 2577.

19 T. Xie, J. M. Bowman, *Chem. Phys. Lett.* **2005**, *412*, 131.

20 B. Hartke, J. Manz, *J. Chem. Phys.* **1990**, *92*, 220.

21 S. Fujita, A. Garcia, *J. Phys. Chem. Solids* **1991**, *52*, 351.

22 Y. Dakhnovskii, B. Bursulaya, H. J. Kim, *J. Chem. Phys.* **1995**, *102*, 7838.

23 B. M. Baer, *Chem. Phys. Lett.* **1999**, *312*, 203.

24 R. T. Hart, Q. Mei, C. J. Benmore, J. C. Neuefeind, J. F. C. Turner, M. Dolgos, B. Tomberli, P. A. Egelstaff, *J. Chem. Phys.* **2006**, *124*, 134505.

25 T. Murakawa, T. Okajima, S. Kuroda, T. Nakamoto, M. Taki, Y. Yamamoto, H. Hayashi, K. Tanizawa, *Biochem. Biophys. Res. Commun.* **2006**, *342*, 414.

26 K. Ando, *J. Chem. Phys.* **2006**, *125*, 014104; K. Ando, *Chem. Phys. Lett.* **2003**, *376*, 532; K. Ando, *Phys. Rev. B* **2005**, *72*, 172104.

27 J. C. Tully, *Annu. Rev. Phys. Chem.* **2000**, *51*, 153.

28 W. H. Miller, *J. Phys. Chem. A* **2001**, *105*, 2942.

29 G. A. Fiete, E. J. Heller, *Rev. Mod. Phys.* **2003**, *75*, 933.

30 J. L. Gao, D. G. Truhlar, *Annu. Rev. Phys. Chem.* **2002**, *53*, 467.

31 M. F. Herman, E. Kluk, *Chem. Phys.* **1984**, *91*, 27.

32 K. G. Kay, *Phys. Rev. A* **1992**, *46*, 1213.

33 G. D. Billing, *Phys. Chem. Chem. Phys.* **2002**, *4*, 2865.

34 M. Ben-Nun, T. J. Martinez, *J. Chem. Phys.* **1998**, *108*, 7244; **2000**, *112*, 6113.

35 C. L. Lopreore, R. E. Wyatt, *Phys. Rev. Lett.* **1999**, *82*, 5190.

36 K. Hotta, K. Takatsuka, *J. Phys. A: Math. Gen.* **2003**, *36*, 4785.

37 I. Burghardt, *J. Chem. Phys.* **2005**, *122*, 094103.

38 R. Jackiw, A. Kerman, *Phys. Lett. A* **1979**, *71*, 158.

39 F. Cooper, S.-Y. Pi, P. N. Stancioff, *Phys. Rev. D* **1986**, *34*, 3831.

40 Y. Tsue, Y. Fujiwara, *Prog. Theor. Phys.* **1991**, *86*, 443.

41 Y. Tsue, *Prog. Theor. Phys.* **1992**, *88*, 911.

42 Y. Shigeta, Y. Ozaki, K. Kodama, H. Nagao, H. Kawabe, K. Nishikawa, *Int. J. Quantum Chem.* **1998**, *69*, 629.

43 Y. Shigeta, H. Takahashi, S. Yamanaka, M. Mitani, H. Nagao, K. Yamaguchi, *Int. J. Quantum Chem.* **1998**, *70*, 659.

44 Y. Shigeta, H. Nagao, K. Nishikawa, K. Yamaguchi, *J. Chem. Phys.* **1999**, *111*, 6171; Y. Shigeta, H. Nagao, K. Nishikawa, K. Yamaguchi, *Int. J. Quantum Chem.* **1999**, *75*, 875.

45 H. Nakai, K. Sodeyama, M. Hoshino, *Chem. Phys. Lett.* **2001**, *345*, 118.

46 H. Nakai, *Int. J. Quantum Chem.* **2002**, *86*, 511.

47 H. Nakai, K. Sodeyama, *J. Chem. Phys.* **2003**, *118*, 1119.

48 H. Nakai, M. Hoshino, K. Miyamoto, S. Hyodo, *J. Chem. Phys.* **2005**, *122*, 164101; **2005**, *123*, 237102.

49 K. Sodeyama, K. Miyamoto, H. Nakai, *Chem. Phys. Lett.* **2006**, *421*, 72.

50 M. Hoshino, H. Nakai, *J. Chem. Phys.* **2006**, *124*, 194110.

51 K. Miyamoto, M. Hoshino, H. Nakai, *J. Chem. Theory Comput.* **2006**, *2*, 1544.

52 K. Sodeyama, H. Nishizawa, M. Hoshino, M. Kobayashi, H. Nakai, *Chem. Phys. Lett.* **2007**, *433*, 409.

53 Y. Imamura, H. Kiryu, H. Nakai, *J. Comput. Chem.* **2008**, *29*, 735.

54 M. Tachikawa, K. Mori, H. Nakai, K. Iguchi, *Chem. Phys. Lett.* **1998**, *290*, 437.

55 M. Tachikawa, *Chem. Phys. Lett.* **2002**, *360*, 494.

56 T. Ishimoto, M. Tachikawa, M. Yamauchi, H. Kitagawa, H. Tokiwa, U. Nagashima, *Chem. Phys. Lett.* **2003**, *372*, 503; T. Ishimoto, M. Tachikawa, M. Yamauchi, H. Kitagawa, H. Tokiwa, U. Nagashima, *J. Phys. Soc. Jpn.* **2004**, *73*, 1775.

57 T. Ishimoto, M. Tachikawa, H. Tokiwa, U. Nagashima, *Chem. Phys.* **2005**, *314*, 231; T. Ishimoto, M. Tachikawa, H. okiwa, U. Nagashima, *J. Phys. Soc. Jpn.* **2005**, *74*, 3112.

58 T. Ishimoto, M. Tachikawa, U. Nagashima, *J. Chem. Phys.* **2006**, *124*, 014112; T. Ishimoto, M. Tachikawa, U. Nagashima, *Int. J. Quantum Chem.* **2006**, *106*, 1465; T. Ishimoto, M. Tachikawa, U. Nagashima, *J. Chem. Phys.* **2006**, *125*, 144103.

59 T. Udagawa, M. Tachikawa, *J. Chem. Phys.* **2006**, *125*, 244105.

60 Y. Itou, S. Mori, T. Udagawa, M. Tachikawa, T. Ishimoto, U. Nagashima, *J. Phys. Chem. A* **2007**, *111*, 261.

61 T. Iordanov, S. Hammes-Schiffer, *J. Chem. Phys.* **2003**, *118*, 9489.

62 M. V. Pak, C. Swalina, S. P. Webb, S. Hammes-Schiffer, *Chem. Phys.* **2004**, *304*, 227.

63 M. V. Pak, S. Hammes-Schiffer, *Phys. Rev. Lett.* **2004**, *92*, 103002.

64 C. Swalina, M. V. Pak, S. Hammes-Schiffer, *Chem. Phys. Lett.* **2005**, *404*, 394.

65 C. Swalina, M. V. Pak, S. Hammes-Schiffer, *J. Chem. Phys.* **2005**, *123*, 014303.

66 A. Reyes, M. V. Pak, S. Hammes-Schiffer, *J. Chem. Phys.* **2005**, *123*, 064104.

67 J. H. Skone, M. V. Pak, S. Hammes-Schiffer, *J. Chem. Phys.* **2005**, *123*, 134108.
68 C. Swalina, M. V. Pak, A. Chakraborty, S. Hammes-Schiffer, *J. Phys. Chem. A* **2006**, *110*, 9983.
69 M. V. Pak, A. Chakraborty, S. Hammes-Schiffer, *J. Phys. Chem. A* **2007**, *111*, 4522.
70 Y. Shigeta, K. Takatsuka, *J. Chem. Phys.* **2005**, *123*, 131101.
71 O. V. Prezhdo, Y. V. Pereverzev, *J. Chem. Phys.* **2000**, *113*, 6557; **2002**, *116*, 4450.
72 E. Pahl, O. V. Prezhdo, *J. Chem. Phys.* **2002**, *116*, 8704.
73 O. V. Prezhdo, *J. Chem. Phys.* **2002**, *117*, 2995.
74 E. Heatwole, O. V. Prezhdo, *J. Chem. Phys.* **2004**, *121*, 10967; **2005**, *122*, 234109; **2007**, *126*, 204108.
75 O. V. Prezhdo, *Theor. Chem. Acc.* **2006**, *116*, 206.
76 H. Miyachi, Y. Shigeta, K. Hirao, *Chem. Phys. Lett.* **2006**, *432*, 585.
77 Y. Shigeta, H. Miyachi, K. Hirao, *J. Chem. Phys.* **2006**, *125*, 244102.
78 Y. Shigeta, H. Miyachi, K. Hirao, *Chem. Phys. Lett.* **2007**, *443*, 414.
79 Y. Shigeta, *J. Chem. Phys.* **2008**, *128*, 161103.
80 J. Florián, V. Hrouda, P. Hobza, *J. Am. Chem. Soc.* **1994**, *116*, 1457.
81 J. Florián, J. Leszczyn'sky, *J. Am. Chem. Soc.* **1996**, *118*, 3010.
82 G. Villani, *Chem. Phys.* **2005**, *316*, 1; G. Villani, **2006**, *324*, 438.
83 T. Matsui, Y. Shigeta, K. Hirao, *Chem. Phys. Lett.* **2006**, *423*, 331; T. Matsui, Y. Shigeta, K. Hirao, *J. Chem. Phys. B* **2007**, *111*, 1176.
84 K. Yagi, C. Oyanagi, T. Taketsugu, K. Hirao, *J. Chem. Phys.* **2003**, *118*, 1653.
85 K. Yagi, K. Hirao, T. Taketsugu, M. W. Schmidt, M. S. Gordon, *J. Chem. Phys.* **2004**, *121*, 1383.
86 E. Wigner, *Phys. Rev.* **1932**, *40*, 749.
87 R. P. Feynman, A. R. Hibbs, *Quantum Mechanics and Path Integrals*, McGraw-Hill, New York, **1965**.
88 R. P. Feynman, H. Kleinert, *Phys. Rev. A* **1986**, *34*, 5080.
89 B. Winstead, H. Tsuchiya, U. Ravaioli, *J. Comput. Electron.* **2002**, *1*, 201.
90 A. Horikoshi, private communication.
91 Y. Nambu, *Phys. Rev. D* **1973**, *7*, 2405.